PAPER

From a reflectrometry code to a 'standard' EC code to investigate the impact of the edge density fluctuations on the EC waves propagation

View the article online for updates and enhancements.

IOP ebooks™

Bringing you innovative digital publishing with leading voices to create your essential collection of books in STEM research.

Start exploring the collection - download the first chapter of every title for free.

From a reflectrometry code to a 'standard' EC code to investigate the impact of the edge density fluctuations on the EC waves propagation

N Bertelli, G J Kramer and E J Valeo

Princeton Plasma Physics Laboratory, Princeton, NJ 08540 United States of America

E-mail: nbertell@pppl.gov

Abstract

In this work we employ and extend a 2D/3D code (FWR2D/FWR3D), originally developed for reflectrometer simulations, to study the impact of the edge density fluctuations on the electron cyclotron (EC) wave beam propagation. 2D and 3D simulations for DIII-D-like plasma are discussed with and without the presence of the edge density fluctuations in order to evaluate the impact on the EC wave beam broadening at the location of the EC resonance. Moreover, a comparison between the paraxial and the full-wave solution (which are both implemented in the code, making it very flexible) of the EC beam with and without edge density fluctuations is shown. The paraxial solution is numerically convenient and in very good agreement with the full-wave solution. A scan in the amplitude of edge density fluctuations is performed together with an average with 1000 different fluctuations realizations. For the case shown in this work, an ensemble larger than 100 independent edge density fluctuations shows to reasonably represent the impact of the fluctuations on the EC beam. Our simulations shown here demonstrate the importance of the edge density fluctuations to the EC propagation in agreement with previous work.

Keywords: EC waves, edge density fluctuations, full-wave, paraxial solution

(Some figures may appear in colour only in the online journal)

1. Introduction

The importance of the interaction of radio-frequency (RF) waves with the scrape-off layer (SOL) is one of the important research areas in these recent years. All RF actuators in different frequency regimes (ion cyclotron, lower hybrid, and electron cyclotron (EC)) can be affected by the presence of the SOL plasma in terms of propagation and coupling. Several experimental and modeling studies were published for ion cyclotron and lower hybrid heating and current drive schemes ([1, 2] and reference within). As for the EC regime, a series of modeling studies have been recently published on the EC wave beam propagation in the presence of edge density fluctuations [3–15]. These works show that the SOL density fluctuations can affect the EC beam propagation and

causing a possible power deposition broadening. Such a broadening, particularly, at the location of the EC resonance in the plasma could, in principle, reduce the EC current drive efficiency that is needed to stabilize/suppress neoclassical tearing modes (NTMs) [8, 16–18]. A recent experimental study shows a direct measurement of the scattering of a millimeter-wave beam by plasma blobs in the TORPEX device [19, 20] while on the TCV tokamak similar effects were found [21, 22]. Brookman *et al* reported on an initial experimental confirmation of broadened ECH deposition also on DIII-D tokamak [23]. It is clear from the number of publications in this research area, how important it is to predict the EC propagation in particular for experiments such as ITER. Generally, the standard EC codes used in the community such as, for instance, GENRAY [24, 25], GRAY
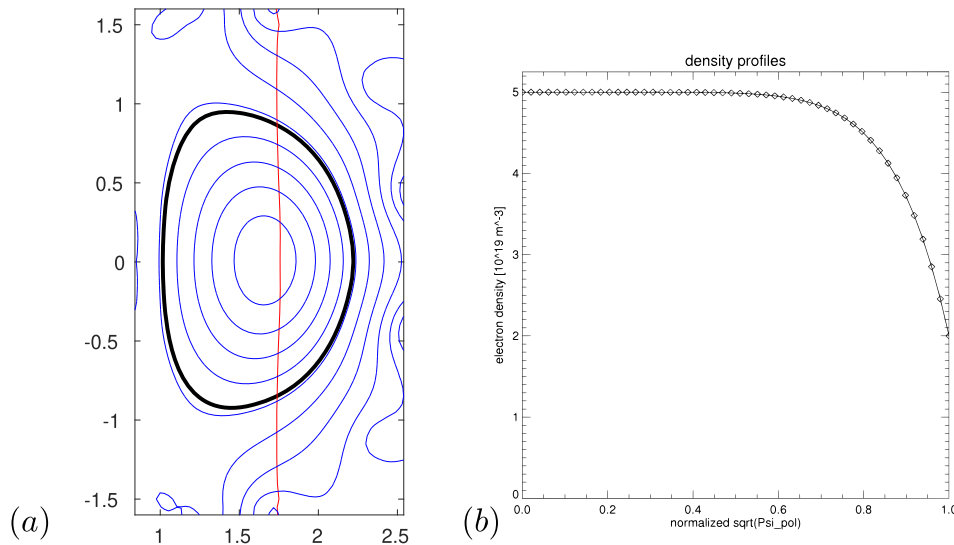
Figure 1. (a) Magnetic flux surfaces equilibrium used in the simulations. The bold black curve represents the last closed flux surface and the red line is the 2nd electron cyclotron harmonic. (b) The electron density as a function of the square root of the normalized poloidal flux.

[26], TORAY [27–29], TORBEAM [30, 31], and TRAVIS [32] have been developed initially to evaluate the power deposition and the current drive profiles in the plasma without considering edge density fluctuations. More recently, a series of numerical tools, have been developed WKBeam[33], IPF-FDMC [34], EMIT-3D [35], COMSOL [22] and [7, 10] with the ability to include a scattering model representing the effect of edge density flunctuations. These tools have been developed with different techniques and approximation therefore the reader is referred to the references for more details. In this work we show here two new numerical tools, FWR2D and FWR3D, originally developed for reflectometer simulations [36, 37] to address the impact of the edge turbulence on the EC propagation. These codes were commonly used for reflectometer antenna-plasma coupling calculations that include density fluctuations and also for interpreting the experimental data [38–41]. These codes have a series of useful and powerful capabilities, among them: (i) FWR2D and FWR3D solve the Maxwell equations in both 2D and 3D geometries, respectively, including the edge density fluctuations; (ii) the numerical domain is divided in three regions: a vacuum region, a paraxial region, and a full-wave region, each with the appropriate wave solving strategy for high computation efficiency. The size of these regions are set by the user to maximize the numerical efficiency. It is quite evident that such capabilities are ideal for studying the impact of the edge density fluctuation on EC propagation.

In this work we briefly introduce FWR2D and FWR3D code and we show some of their applications in both 2D and 3D geometries with and without edge density fluctuations. In particular, this paper is structured as follows: in section 2, a brief description of the code is presented together with the density fluctuations model implemented in the code. Section 3 shows the plasma scenario (DIII-D-like plasma) adopted in the numerical calculations. In section 4, a comparison between the full-wave and paraxial solutions of the EC beam

with and without edge density fluctuations is shown and discussed. Section 5 shows a scan in the amplitude of edge density fluctuations with different fluctuations correlation length. Moreover, a convergence test is discussed assuming several realization of the edge density fluctuations. In section 6, a few 3D applications are presented and a comparison with the 2D cases is also discussed. Finally, section 7 contains a discussion and a summary of the work presented here.

2. The FWR2D and FWR3D codes

FWR2D is a two-dimensional wave propagation code, developed specifically to simulate correlation reflectometry in large-scale fusion plasmas [36]. In this code the computational domain is divided into three regions: (i) a vacuum region, (ii) a paraxial region, and (iii) a full-wave region. This code was developed for reflectometry studies and its hybrid approach is so able to be computational efficient and at the same time to use the full-wave model near the reflection layer where the paraxial approach and ray tracing break down. Moreover, the computational domain is fully set by the user therefore one can have a computational domain just big enough to include the EC beam. The code allows to set also an additional collisional damping on the boundary of the computational domain to avoid possible reflection. An antenna is specified at a plane outside the plasma providing the wave field pattern. In the vacuum region the waves propagate from the antenna to the plasma edge by making use of the free-space Greens function to project the wave field between the antenna and plasma boundary. Between the edge plasma and the surface close to the refection layer FWR2D is using the paraxial technique to solve the wave equation [36, 41–44]. At the boundary between the paraxial and the full-wave region, the incoming paraxial solution is used to construct the source for the full-wave
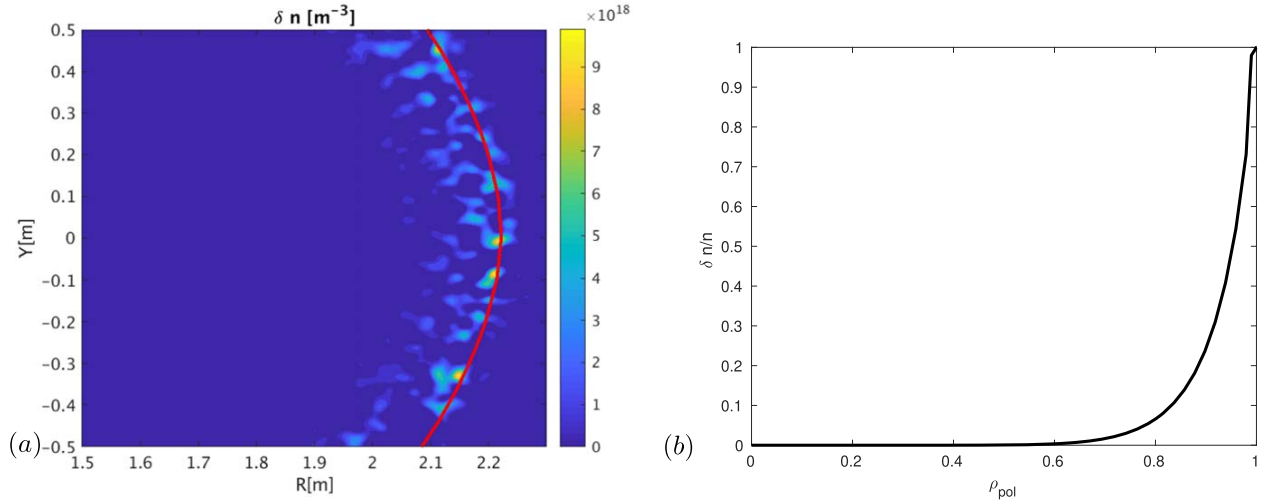
Figure 2. (a) 2D density fluctuations used in the simulations where the red curve represents the last closed flux surface. (b) The normalized density fluctuations as a function of the square root of the normalized poloidal flux.

solution. In the full-wave region the code solves the 2D wave equation [36]

$$(\nabla^2 + k_0^2 \varepsilon(x, y))E(x, y, t) + 2i\frac{\omega}{c^2}\frac{\partial E(x, y, t)}{\partial t} = 0 \quad (1)$$

until a steady state solution $(\partial E(x, y, t)/\partial t = 0)$ is reached (assuming a full time-space variation given as $\mathcal{E}(x, y, t) = E(x, y, t)e^{-i\omega t}$ [36]). In equation (1), $E(x, y, t)$ represents the wave electric field as a function of space (x, y) and time t; $k_0 \equiv \omega/c$ is the wave vector in free-space. The dielectric tensor, ε, implemented in the code is the magnetized cold plasma X- or O-mode dielectric [45] including the relativistic corrections [40, 46–48]. The model includes a realistic antenna radiation pattern and the capability to input experimentally inferred two-dimensional profiles of density, electron temperature and magnetic field strength. FWR2D has been generalized to 3D geometry with a code named FWR3D [37].

In FWR2D a time-dependent random density field is implemented in the code where each time slice represents a two-dimensional random density distribution drawn from a distribution with the following spectral properties [39]:

$$\frac{\langle \tilde{n}_1 \tilde{n}_2 \rangle}{n^2} = \left(\frac{\tilde{n}}{n}\right)^2 \exp\left[-\left(\frac{\Delta t}{\tau}\right)^2\right]$$

$$\times \exp\left\{-\left[\frac{(\mathbf{x} + \mathbf{v}t) \cdot \Delta\mathbf{k}}{2}\right]^2\right\}\cos(\mathbf{x} \cdot \mathbf{k}), \quad (2)$$

where $\tilde{n}/n$ is the density fluctuation level, which can depend on the radial position (as in this work), τ is the density de-correlation time, $\mathbf{v}$ is the poloidal velocity of the turbulence, $\mathbf{k}$ is the mean value of the fluctuation wave number, $\Delta\mathbf{k}$ represents its spread, and $x = (x_1 - x_2, y_1 - y_2)$, with $x_1 - x_2$ and $y_1 - y_2$ the radial and the poloidal displacement, respectively.

For FWR3D, the random density distribution shown in equation (2) is generalized to include the third dimension. The
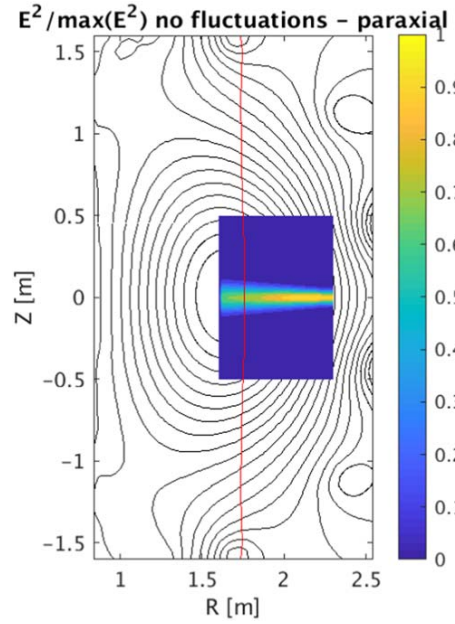

Figure 3. The EC divergent beam propagation with the magnetic flux surfaces in black and the 2nd EC harmonic in red.

fluctuations are aligned to the equilibrium magnetic field in accordance with the experimental observations. These codes have been used extensively for reflectometry studies, to develop synthetic diagnostics and they have been compared to experimental data [36–39, 41, 49, 50].

In this work, we want to take advantages of FWR2D and FWR3D codes to extend their applications to the study of the EC propagation in plasma and not only for reflectometry studies. Indeed all the features described above are ideal for studying the impact of the edge density fluctuations to the EC wave propagation. In our case, the computational
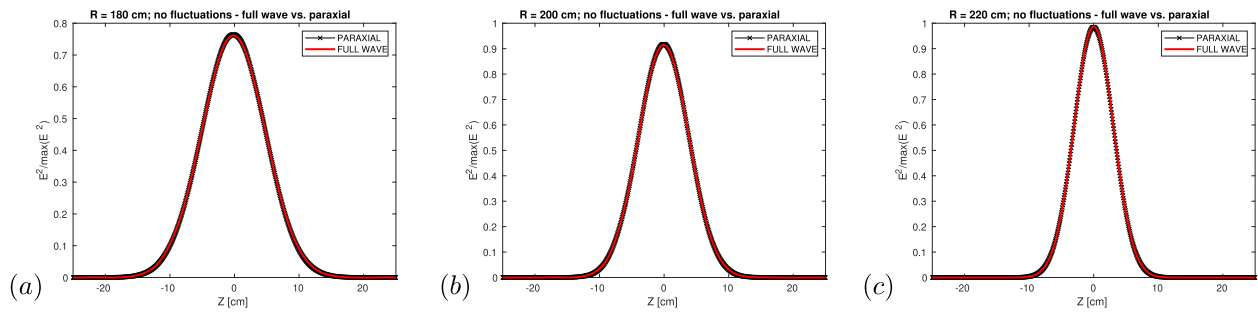
Figure 4. Comparison between paraxial (black curve) and full-wave (red curves) methods of the beam cross-sections at three different radial locations, i.e. $R = 180$ cm (figure (a)), $R = 200$ cm (figure (b)), and $R = 220$ cm (figure (c)).
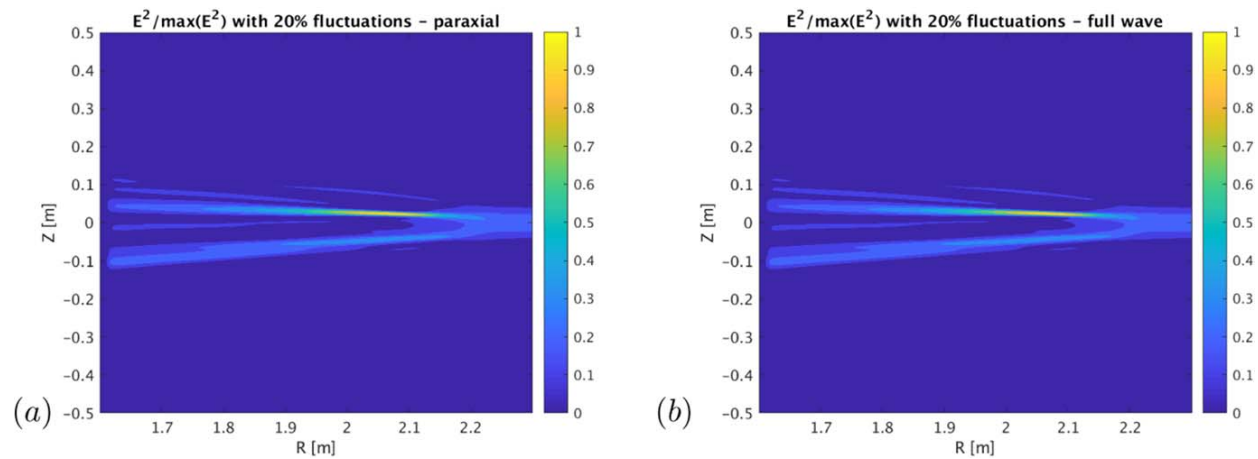
Figure 5. 2D EC beam propagation evaluated by the paraxial (figure (a)) and the full-wave (figure (b)) methods in the presence of the density fluctuations shown in figure 2 with $\max(\delta n/n) = 20\%$.
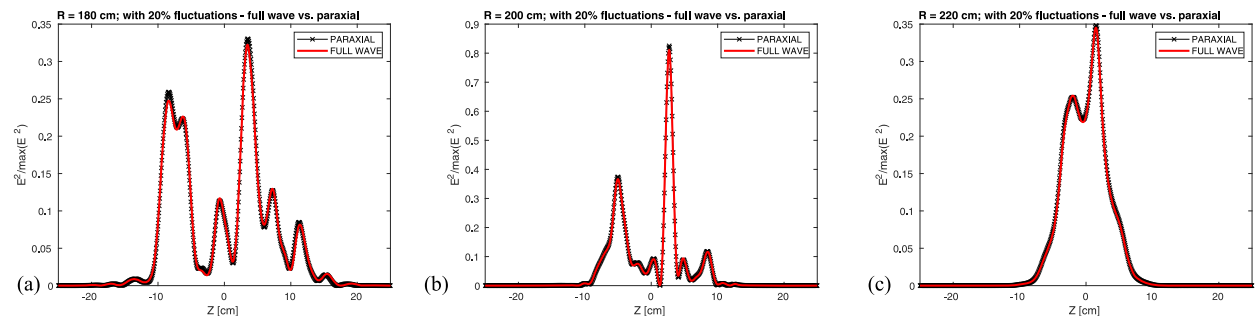

Figure 6. Comparison between paraxial (black curves) and full-wave (red curves) methods of the beam cross-sections with the presence of the density fluctuations at three different radial locations, i.e. $R = 180$ cm (figure (a)), $R = 200$ cm (figure (b)), and $R = 220$ cm (figure (c)).

domain will be divided into two regions: (i) a vacuum region and (ii) a paraxial region or a full-wave region, according with which method the user wants to solve the wave equation. Moreover, unlike the original version of the codes where the turbulence was uniform through the plasma, here the turbulence is a function of the radial coordinate and mainly localized at the plasma edge (see next section). A few applications are discussed in the next sections for a DIII-D-like plasma showing both the paraxial and the full-wave solutions.

3. DIII-D-like scenario considered

The plasma scenario used in this paper is shown in figure 1(a). This figure shows the magnetic flux surfaces of a DIII-D-like plasma where the bold black curve represents the last closed flux surface and the red line indicates the second EC resonance assuming a wave frequency $f = 110$ GHz. For this specific case the EC resonance is located at the low field side. The magnetic field at the magnetic axis is $B = 2$ T. Figure 1(a) shows the electron density profile as a function of
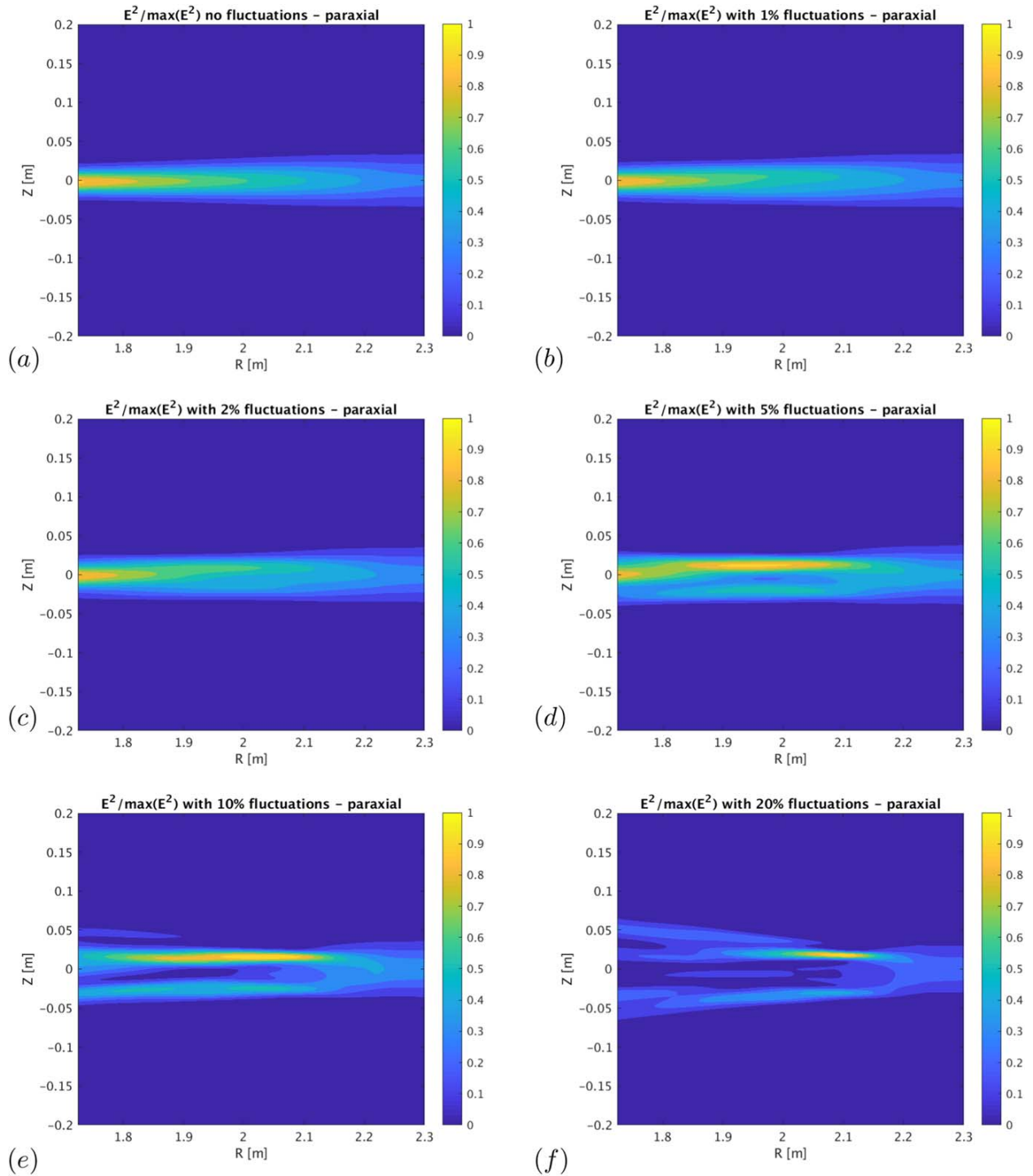
Figure 7. 2D EC beam propagation with no density fluctuations in figure (a) and different density fluctuations with maximum values of 1% (figure (b)), 2% (figure (c)), 5% (figure (d)), 10% (figure (e)), and 20% (figure (f)).

the square root of the normalized poloidal flux, ρ_{pol}. The central density is $n_{\mathrm{e}}(0) = 5.0 \times 10^{19}$ m^{-3} and the edge density at $\rho_{pol} = 1$ is $n_{\mathrm{e}}(1) = 2.0 \times 10^{19}$ m^{-3}. The density profile in the SOL is described by an exponential decay from the LCFS as a function of ρ_{pol} with an e-folding length of 0.03 m.

In this paper we assume the following parameters for the edge density fluctuations with respect equation (2): $\Delta t = 0$ s, $\mathbf{v} = (0, 0)$ m s^{-1}, $\mathbf{k} = (0, 0)$ cm^{-1}, and $\Delta k = (1, 1)$ cm^{-1}. Figure 2(a) shows a single δn realization adopted in the simulations described below when a density fluctuations is included. Moreover, figure 2(b) shows the density

fluctuations, $\delta n/n$, as a function of the square root of the normalized poloidal flux, $\rho_{\rm pol}$. We assume an increase of the density fluctuations from the core plasma towards the edge plasma as generally observed in the experiments [51, 52]. However, in this specific work, we are not aiming to represent exactly the experimental profile of the density fluctuations. The main aim is to show the new numerical tool and its capabilities for a given profile as shown in figure 2 and its possible impact on the EC beam propagation.

4. Paraxial versus full-wave solutions

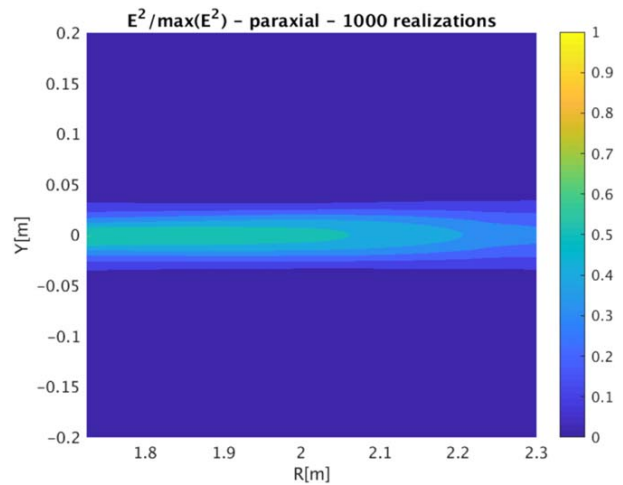### 4.1. No density fluctuations

A comparison between the paraxial and full-wave solutions is discussed with and without density fluctuations for the plasma scenario described in section 3. Figure 3 shows the EC beam propagation without any density fluctuations assuming $f = 110\,{\rm GHz}$ with X-mode polarization, a Gaussian beam with 5 cm beam width, and a focal length $=100\,{\rm cm}$ in order to have a divergent beam. An equatorial launcher as described in section 2. In figure 3 one can easily identify the numerical domain adopted in the simulation in order to minimize the execution time with respect to the entire plasma cross-section. On the left-hand side, top and bottom of the numerical domain a strong absorption is introduced to avoid any possible reflection of outgoing waves (in this specific case, only a reflection from the left-side domain can be expected). Moreover, no EC absorption on the EC resonance is evaluated in FWR2D. Figure 3 shows the square of the amplitude of the electric field normalized to its maximum, $E^2/\max(E^2)$ obtained with the paraxial approximation implemented in the code. We also performed the same simulation with the full-wave approach and a comparison is shown in figure 4. In this figure, the beam cross-sections at three different radial locations ($R = 180$, 200, and 220 cm) are shown comparing the full-wave (red curves) and the paraxial solutions (black curves). One can note that the agreement is excellent, in fact the curves are basically indistinguishable.

4.2. With density fluctuations

A similar comparison between paraxial and full-wave solutions is also shown in figures 5 and 6 in the presence of the density fluctuations. The maximum value of the edge density fluctuations is here $\frac{\tilde{n}}{n} = 20\%$. Figures 5(a) and (b) show $E^2/\max(E^2)$ obtained by the paraxial and the full-wave methods, respectively. One can see an excellent agreement between the two methods even in the presence of the edge density fluctuations. Moreover, one can clearly see that the the edge density fluctuations can affect significantly the EC beam propagation. In order to compare even better the two methods, as done similarly above, the beam cross-sections at three different radial locations ($R = 180$, 200, and 220 cm) are shown in figure 6. Again, the paraxial solutions overlap almost exactly the full-wave solutions.
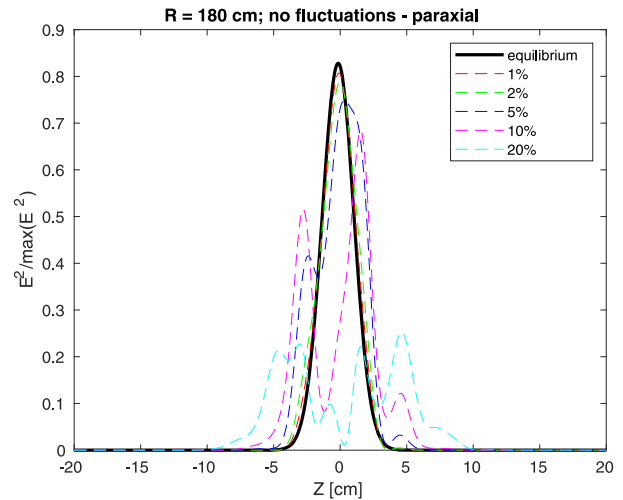
Figure 8. Beam cross-section for the cases shown in figure 7 at $R = 180$ cm. The bold black curve represents the equilibrium case.


Figure 9. Averaged EC propagation assuming 1000 different realizations of the density fluctuations (with $\max(\delta n/n) = 10\%$) to be compared with the equilibrium case shown in figure 7(a).

In this section we have showed an example with reasonable plasma fluctuations parameters in order to emphasize the code capability. However, it is well-know that the paraxial technique implemented in the code may fail in the presence of short scale fluctuations, i.e. in this specific case, large value of Δk_y (see equation (2)).

5. Density fluctuations scan and convergence test

In the results shown in the previous section, we assume a single value for the edge density fluctuations and also a single realization. In this section, instead, we perform a scan of the amplitude of the density fluctuations in order to see the behavior of the EC beam propagation by using the paraxial
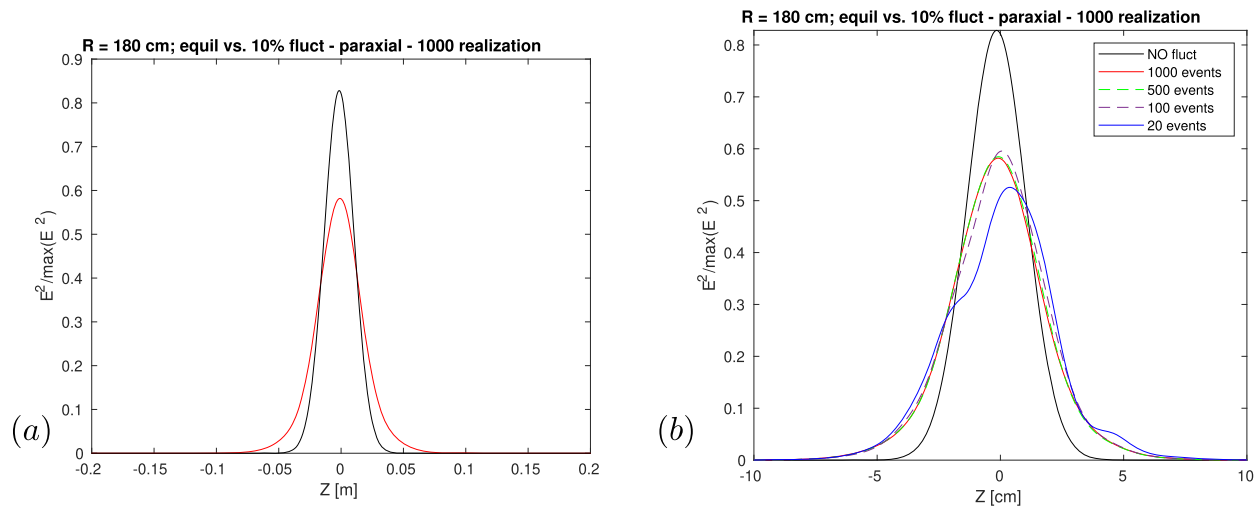
Figure 10. (a) Comparison of the beam cross-section at $R = 180$ cm between the case without fluctuations (black curve) with the averaged solution when 1000 different realization of the density fluctuations are adopted. (b) Convergence test of the average solutions with different number of realizations of density fluctuations (20, 50, 100, 500, and 1000 realizations).

approximation. In these simulations a focusing beam is used and and statistical ensemble of density fluctuations up to 1000 is used. A varying ensemble size is also used to study the power deposition convergence near the EC absorption layer.

### 5.1. Density fluctuations scan

A density fluctuation scan is shown in figure 7 for five different maximum values of amplitude of the edge density fluctuations (1%, 2%, 5%, 10%, and 20%). Unlike in the previous section, a focusing beam is assumed in these simulations to be more consistent with real experiments. Beam parameters are the same as used above except for the focal length, which is -100 cm in this case. All these simulations are performed with the parameters described in section 3 and with the paraxial approximation only because the full-wave approach provides exactly the same results (section 4). From figure 7 one can see that the EC beam propagation is affected by the edge density fluctuations and their effects are stronger for larger density fluctuations as expected. Moreover, due to the edge density fluctuations the EC beam broadens as propagates and more dramatically it can split into different beams. Figure 8 shows, the beam cross-section at $R = 180$ cm where one can clearly see the impact of the fluctuations on the EC beam footprint. In the figure the black curve represents the case without edge density fluctuations whereas the color dashed-curves indicate the $E^2/\max(E^2)$ for the five different amplitude of the edge density fluctuations (1%, 2%, 5%, 10%, and 20%). In this specific scan, one single realization for the density fluctuations was used. In order to make meaningful conclusions on the impact of the density fluctuations on the EC beam propagation an statistical ensemble of realizations of the edge density fluctuations is needed. This is shown in the next subsection.
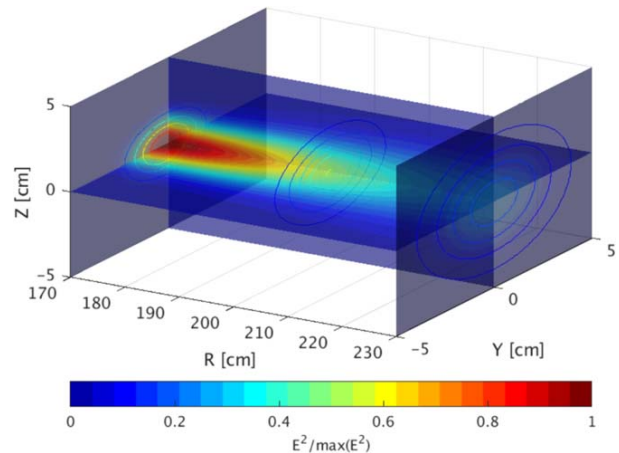
Figure 11. 3D EC beam propagation evaluated by the FWR3D with the paraxial approximation without edge density fluctuations. Same beam parameter used in the 2D calculation.

5.2. Convergence test

Figure 9 shows $E^2/\max(E^2)$ averaged over 1000 realizations of the edge density fluctuations using a value of the density fluctuations 10% . Compared to figure 7(a) the EC beam is broadened in the plasma although the individual realization scatters significantly the average deposition profile (see figure 7(e)) In order to better visualize the broadening with respect to the equilibrium case, figure 10(a) shows $E^2/\max(E^2)$ at $R = 180$ cm with (red curve) and without (black curve) fluctuations. Furthermore, a convergence test based on different numbers of realizations is shown in figure 10(b). This figure shows that an statistical ensemble larger than 100 realizations one can get a reasonable representation of the impact of the edge density fluctuations on the EC beam propagation. In figure 10(b) it is shown the
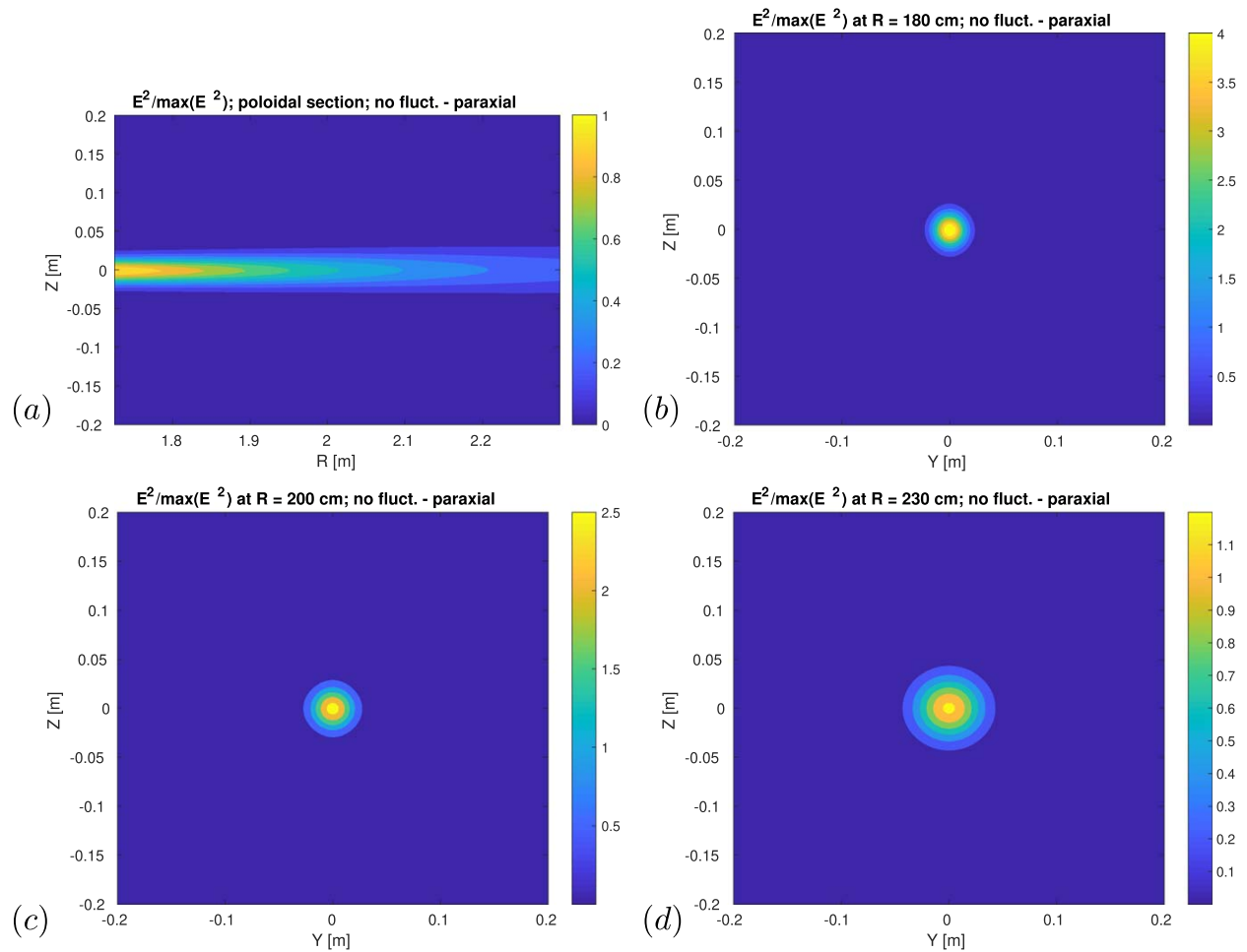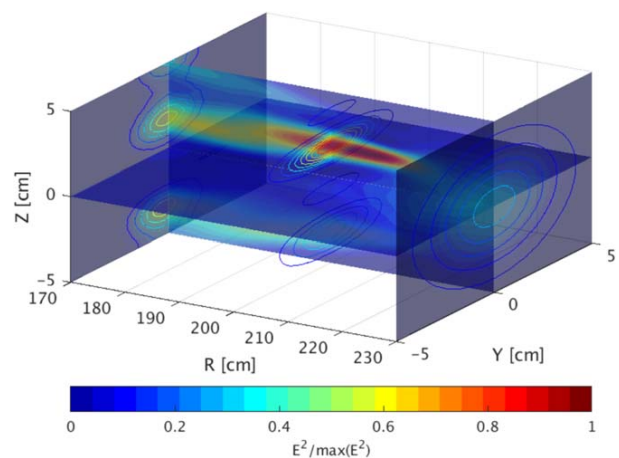
Figure 12. (a) Poloidal section of the 3D EC beam shown in figure 11; cross-sections of the EC beam at three different loations: $R = 180$ cm (b), $R = 200$ cm (c), $R = 230$ cm (d).

equilibrium case (black curve) and four cases: 20, 50, 100, 500, and 1000 realizations.

6. Extension to the 3D geometry with the FWR3D code

A 3D version (named FWR3D) of the well established 2D hybrid simulation code, FWR2D, was developed [37], as described in section 2. In this section we apply the FWR3D code for the case shown in the previous section. Figure 11 shows the focusing EC beam in 3D geometry using the same parameters employed in the previous section without edge density fluctuations. In particular, figure 12 shows the corresponding poloidal cross-section of the EC beam propagation together with three different beam cross-sections at three different locations along the beam propagation ($R = 180$, 200, and 230 cm). From these figures we can note the circular cross-section represented by an initial Gaussian

Figure 13. 3D EC beam propagation evaluated by the FWR3D with the paraxial approximation with edge density fluctuations ($\max(\delta n/n) = 20\%$). Same beam parameter used in the 2D calculation.
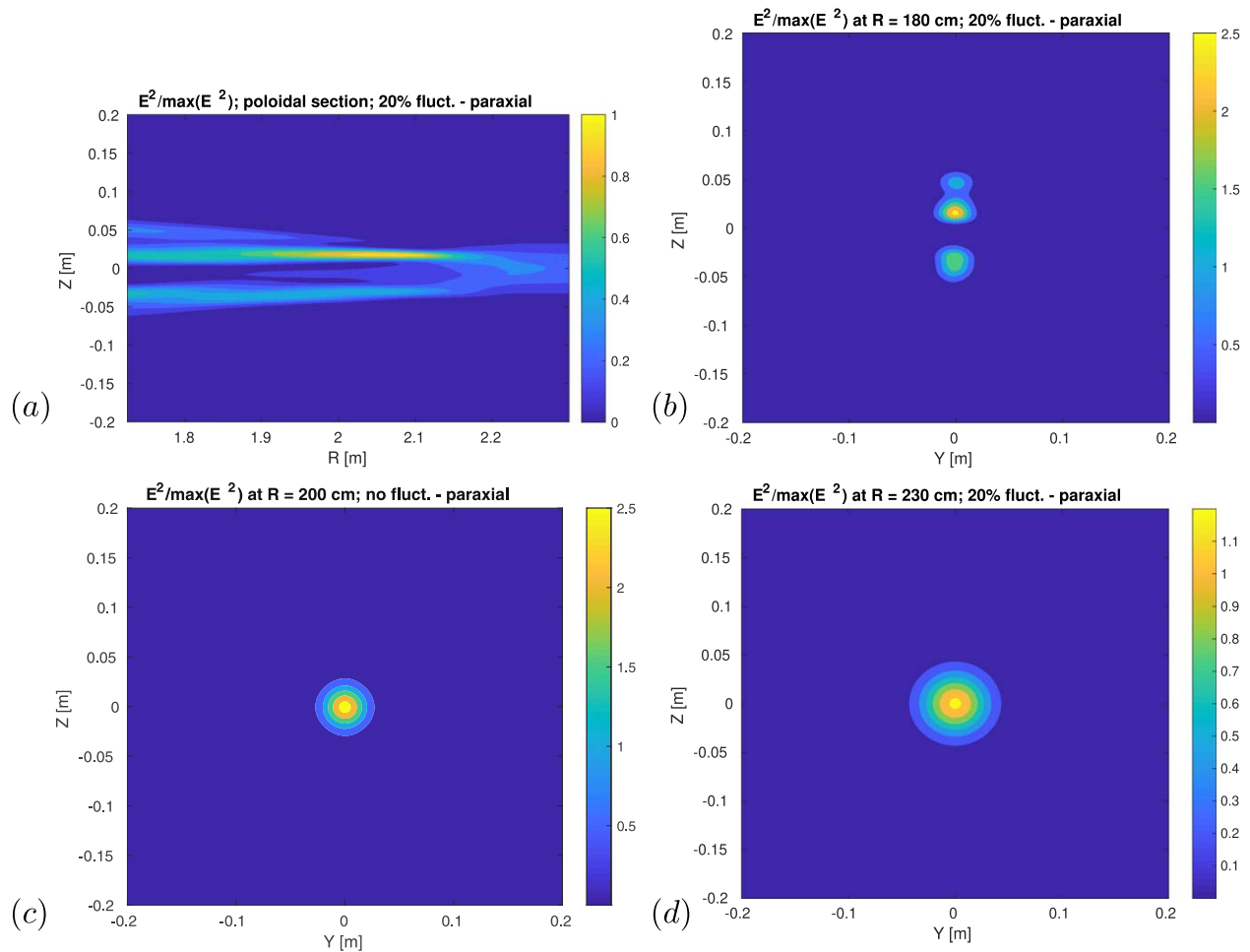
Figure 14. (a) Poloidal section of the 3D EC beam shown in figure 13; cross-sections of the EC beam at three different locations: $R = 180$ cm (b), $R = 200$ cm (c), $R = 230$ cm (d).

beam (figure 12(d)) with the focusing at lower R (figures 12(b) and (c)). Moreover, it is important to compare figures 12(a) with the figure 7(a) that was obtained with the 2D code. These two figures show very similar results. In other words, the 3D results are consistent with the 2D results. A more quantitative comparison is shown in figure 15(a) where the beam cross-section at $R = 180$ cm evaluated by both FWR2D (dashed-balck curve) and FWR3D (red curve) is plotted. A very good agreement is evident for this case.

In the presence of the edge density fluctuations the EC beam splits into several beamlets as shown in figure 13 with $\max(\delta n/n) = 20\%$. For this specific case, the edge density fluctuations were taken in the toroidal direction instead of field- aligned in order to be able to compare our 3D results with the 2D results. In reality, the code generally takes the density perturbation along the direction of the equilibrium magnetic field (see section 2). Figure 13 shows that the initial EC Gaussian beam is split into two sub-beams due to the edge fluctuations and this splitting occurs vertically along the z-axis. A tilt angle would have been occurred if the density fluctuations were taken to be along the equilibriuml magnetic field line and not purely in the toroidal direction [41]. A more

clear visualization is given in the figure 14 as analogously done for the case without edge fluctuations. Figures 14(d) shows the initial Gaussian EC beam whereas figures 14(b) and (c) show the splitting beam due to the fluctuations. It is important to note that the beam is split along the vertical z-axis because the edge density fluctuations are taken in the toroidal direction (y-axis). Figures 7(f) and 14(a) show a qualitative good agreement. In figure 15, one can see clearly the difference of the beam cross-sections evaluated by the 2D (dashed black curve) and the 3D (red curve) codes. The shape of the profiles is quite similar but differences in the field amplitude clearly appear.

7. Discussion and conclusions

In this work we have showed a new numerical tool together with its capabilities to study the impact of the edge density fluctuations to the EC wave propagation. Such effect has been shown to be important from both previous modeling and observations. This code has been originally developed for reflectometry studies and it is a 'hybrid code' because the
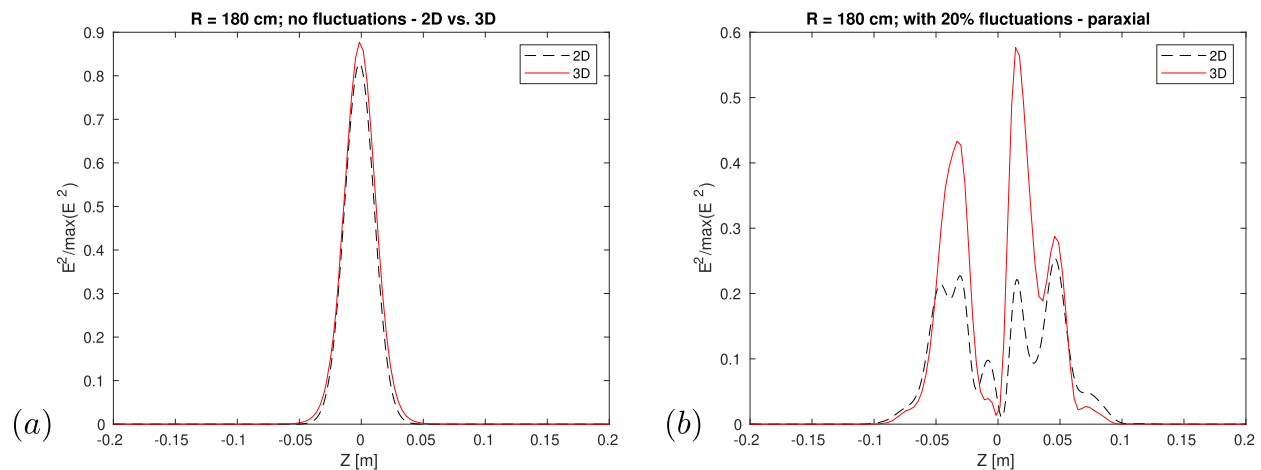
Figure 15. (a) Comparison between the beam cross-section evaluated by the 2D (dashed black curve) and the 3D (red curve) codes at $R = 180$ cm and $Y = 0$ cm for the case without fluctuations (20%); (b) comparison between the beam cross-section evaluated by the 2D (dashed black curve) and the 3D (red curve) codes at $R = 180$ cm for the case with fluctuations (20%).

numerical domain can be divided into three regions: (i) a vacuum region; (ii) a paraxial region; and (iii) a full-wave region. It incorporates an edge density fluctuation model and it solves the Maxwell equations in 2D and 3D. All of these features are ideal for studying the standard EC propagation in the presence of the edge density fluctuations. In this paper we have adopted a DIII-D-like plasma scenarios using an EC beam. We found an excellent agreement between the paraxial and the full-wave methods with and without the presence of the edge density fluctuations. A scan of the amplitude of the edge density fluctuations has been discussed showing a clear impact of the edge density fluctuations on the EC beam propagation. Moreover, a large ensemble of independent edge density fluctuations (1000) has been generated and used to evaluate the impact of the edge density fluctuations on the broadening of the EC beam. A clear broadening is found with a 10% relative amplitude of the density fluctuations. A statistical ensemble larger than 100 edge density fluctuations has been shown to reasonably represent the impact of the edge density fluctuations on the EC beam. However, this number is based on the specific applications shown in this work. Finally, the 3D capability of FWR3D has been shown. In particular, the 3D extension of the 2D results has been discussed showing that the 3D geometry can be important for studying the effect of the fluctuations. In general, our work agrees with previous works showing that indeed the edge fluctuations can affect the EC beam propagation and this can have a consequence mainly for the NTM suppression [4, 8, 13–15, 17]. FWR2D and FWR3D could be used for extensive comparisons with experiments and other independent codes. Currently FWR2D and FWR3D assume only the propagation near and parallel to the midplane (useful for reflectometry) and no anti-hermitian part of the dielectric tensor is implemented in the code, therefore no information about the power absorption and current drive can be calculated. These extension/generalization will be implemented in the future. Nevertheless, we believe that such a tool and its versatility together with the results presented here can be useful for a

comparison with experimental data with the possibility to incorporate realistic edge density fluctuations measured from the experiment and analytical model [9] when possible. Moreover, a possibility of using this code with the edge density fluctuations obtained by transport codes is also planned and it will be part of a future work.

ORCID iDs

N Bertelli ⬡ https://orcid.org/0000-0002-9326-7585
G J Kramer ⬡ https://orcid.org/0000-0001-5105-8139

References

[1] Bonoli P T 2014 *Phys. Plasmas* **21** 061508
[2] Wilson J R and Bonoli P T 2015 *Phys. Plasmas* **22** 021801
[3] Tsironis C *et al* 2009 *Phys. Plasmas* **16** 112510
[4] Bertelli N *et al* 2010 *J. Phys.: Conf. Ser.* **260** 012002
[5] Balakin A A *et al* 2011 *IEEE Trans. Plasma Sci.* **39** 3012
[6] Peysson Y *et al* 2011 *Plasma Phys. Control. Fusion* **53** 124028
[7] Ram A K *et al* 2013 *Phys. Plasmas* **20** 056110
[8] Poli E *et al* 2015 *Nucl. Fusion* **55** 013023
[9] Sysoeva E V *et al* 2015 *Nucl. Fusion* **55** 033016
[10] Ram A K and Hizanidis K 2016 *Phys. Plasmas* **57** 022504
[11] Köhn A *et al* 2016 *Plasma Phys. Control. Fusion* **58** 105008
[12] Ioannidis Z C *et al* 2017 *Phys. Plasmas* **24** 102115
[13] Snicker A *et al* 2018 *Nucl. Fusion* **58** 016002
[14] Snicker A *et al* 2018 *Plasma Phys. Control. Fusion* **60** 014020

[15] Köhn A *et al* 2018 *Plasma Phys. Control. Fusion* **60** 075006
[16] La Haye R J 2006 *Phys. Plasmas* **13** 055501
[17] Sauter O *et al* 2010 *Plasma Phys. Control. Fusion* **52** 025002
[18] Bertelli N *et al* 2011 *Nucl. Fusion* **51** 103007
[19] Chellaï O *et al* 2018 *Phys. Rev. Lett.* **120** 105001
[20] Furno I *et al* 2015 *J. Plasma Phys.* **81** 345810301
[21] Chellaï O *et al* 2017 *EPJ Web Conf.* **157** 03008
[22] Chellaï O *et al* 2019 *Plasma Phys. Control. Fusion* **61** 014001
[23] Brookman M W 2017 *EPJ Web Conf.* **147** 03001
[24] Harvey R *et al* 1994 *Bull. Am. Phys. Soc.* **39** 1626
[25] Bertelli N *et al* 2012 *Phys. Plasmas* **19** 082510
[26] Farina D 2007 *Fusion Sci. Technol.* **52** 154
[27] Kritz A H *et al* 1982 *Conf. Proc., 3rd Int. Symp. on Heating in Toroidal Plasmas ECE* vol 2 (Brussels, Belgium) p 769
[28] Matsuda K 1989 *IEEE Trans. Plasma Sci.* **17** 6
[29] Westerhof E 1989 *Implementation of TORAY at JET* Technical Report FOM Institute for Plasma Physics Rijnhuizen, Nieuwegein, The Netherlands
[30] Poli E, Peeters A G and Pereverzev G V 2001 *Comput. Phys. Commun.* **136** 90
[31] Poli E *et al* 2018 *Comput. Phys. Commun.* **225** 36
[32] Marushchenko N B *et al* 2014 *Comput. Phys. Commun.* **185** 165
[33] Weber H *et al* 2015 *EPJ Web Conf.* **87** 01002
[34] Köhn A *et al* 2008 *Plasma Phys. Control. Fusion* **50** 085018

[35] Williams T R N *et al* 2014 *Plasma Phys. Control. Fusion* **56** 075010
[36] Valeo E J *et al* 2002 *Plasma Phys. Control. Fusion* **44** L1
[37] Valeo E J *et al* 2009 *AIP Conf. Proc.* **1187** 649
[38] Kramer G J *et al* 2002 *Plasma Phys. Control. Fusion* **44** L11
[39] Kramer G J, Nazikian R and Valeo E J 2004 *Plasma Phys. Control. Fusion* **46** 695
[40] Kramer G J *et al* 2006 *Nucl. Fusion* **46** S846
[41] Kramer G J *et al* 2018 *Nucl. Fusion* **58** 126014
[42] Feit M D and Fleck J A 1978 *Appl. Opt.* **17** 3990
[43] Berger R L *et al* 1993 *Phys. Fluids* B **5** 2243
[44] Smirnov A I and Petrov E Y 1999 *Proc. 26th EPS Conf. on Plasma Physics and Controlled Fusion* vol 23J, p 1797
[45] Stix T H 1992 *Waves in Plasmas* (NY: American Institute of Physics)
[46] Mazzucato E 1992 *Phys. Fluids* B **4** 3460
[47] Bindslev H 1992 *Plasma Phys. Control. Fusion* **34** 1601
[48] Bindslev H 1993 *Plasma Phys. Control. Fusion* **35** 1093
[49] Kramer G J, Nazikian R and Valeo E 2003 *Rev. Sci. Instrum.* **74** 1421
[50] Nazikian R *et al* 2005 *Phys. Rev. Lett.* **94** 135002
[51] Fonck R J *et al* 1993 *Phys. Rev. Lett.* **70** 3736
[52] Wesson J 2004 *Tokamaks* 3rd edn (Oxford: Oxford University Press)